Article

Individual Gas Molecules Detection Using Zinc Oxide–Graphene Hybrid Nanosensor: A DFT Study

Ingrid Torres [1], Sadegh Mehdi Aghaei [1],*, Amin Rabiei Baboukani [2], Chunlei Wang [2] and Shekhar Bhansali [1]

[1] Department of Electrical and Computer Engineering, Florida International University,
    Miami, FL 33174, USA; itorr001@fiu.edu (I.T.); sbhansa@fiu.edu (S.B.)
[2] Department of Mechanical and Materials Engineering, Florida International University,
    Miami, FL 33174, USA; arabi009@fiu.edu (A.R.B.); wangc@fiu.edu (C.W.)
* Correspondence: smehd002@fiu.edu; Tel.: +1-305-332-8084

Abstract: Surface modification is a reliable method to enhance the sensing properties of pristine graphene by increasing active sites on its surface. Herein, we investigate the interactions of the gas molecules such as NH_3, NO, NO_2, H_2O, and H_2S with a zinc oxide (ZnO)–graphene hybrid nanostructure. Using first-principles density functional theory (DFT), the effects of gas adsorption on the electronic and transport properties of the sensor are examined. The computations show that the sensitivity of the pristine graphene to the above gas molecules is considerably improved after hybridization with zinc oxide. The sensor shows low sensitivity to the NH_3 and H_2O because of the hydrogen-bonding interactions between the gas molecules and the sensor. Owing to observable alterations in the conductance, large charge transfer, and high adsorption energy; the sensor possesses extraordinary potential for NO and NO_2 detection. Interestingly, the H_2S gas is totally dissociated through the adsorption process, and a large number of electrons are transferred from the molecule to the sensor, resulting in a substantial change in the conductance of the sensor. As a result, the ZnO–graphene nanosensor might be an auspicious catalyst for H_2S dissociation. Our findings open new doors for environment and energy research applications at the nanoscale.

Keywords: graphene; zinc oxide; ZnO; sensor; NH_3; NO; NO_2; H_2S; adsorption; density functional theory (DFT)

1. Introduction

There are presently great efforts being made in developing novel gas sensors centered around new nanomaterials for the detection of toxic gases since they offer higher sensitivity, selectivity, and reliability; as well as immediate response and recovery at low cost. One of the most significant advantages that nanostructure-based sensors have over conventional microsensors is the high surface-to-volume ratio. This is a crucial parameter since it defines the sensitivity of the gas sensors. Moreover, the nanostructured materials provide a greater detection area leading to better adsorption of gas species and an increase in sensing abilities.

Graphene, the first discovered two-dimensional (2D) material, has become a promising material for different types of applications [1,2]. Graphene's amazing properties have attracted considerable interest in the area of gas sensing since they enable the improvement of miniaturized sensors at low cost and power consumption [3–5]. Consequently, graphene has been extensively studied theoretically [6–14] and experimentally [15–20]. On the downside, because of the weak interactions between π electrons of graphene's surface and the gas molecules, pristine graphene has shown limitations for the recognition of individual gas particles [9,10], exhibiting low sensitivity to common

gases such as CO, CO_2, CH_4, N_2, NO_2, NH_3, H_2, and H_2O [6–8]. Therefore, physical or chemical modification of graphene's surface has been considered to boost its performance. Hydrogen plasma [21], reduction reagents [22], and electron beam irradiation [23] are the physical methods that have been applied to modify the surface of the graphene by reducing the graphene oxide (GO). Besides the physical modification, chemical methods such as functionalization, impurity atom doping, and defects have been reported to successfully alter the electrical and magnetic properties of nanomaterials [24–32]. Techniques, where dopants or defects are introduced, have shown an improvement in the sensitivity of the graphene-based gas sensors [7,8,11–14,28–30,33]. Zhang et al. showed small gas molecules such as NO_2, CO, NO, and NH_3 display strong reactions with B-doped, N-doped, and defective graphene [7]. Additionally, when graphene is doped with B, N, and Si, it displayed boosted interactions with other common gases like N_2, SO_2, CO_2, O_2, H_2, and H_2O compared to pristine graphene [8]. Doped graphene with transition metals (Fe, Co, Ni, Ru, Rh, Pd, Os, Ir, and Pt) has also been demonstrated to have high sensitivity to O_2 adsorption [12]. Borisova et al. noticed that when defects are induced on graphene, it improved the interactions of H_2S with C atoms, showing much better response in comparison with pristine graphene [13]. Density functional theory (DFT) calculation on Eu-decorated single- and double-sided graphene sheets exhibited that each Eu could firmly bound to six H_2 molecules [14]. Recently, the sensitivity of other 2D nanomaterials such as MoS_2 [34–36], phosphorene [37,38], hexagonal boron carbide (BC_3) [39,40], WS_2 [41,42], silicene [43–45], and germanene [46] to several gases have been inspected.

Metal oxides like SnO_2, WO_3, etc. have been commonly integrated on gas sensors to improve their performance, specifically their sensitivity and selectivity [47–52]. However, these types of sensors have a significant constraint since they need to operate at high temperatures, between 200–600 °C, limiting their application and integration as well as presenting energy consumption issues and risks of gas explosion. Recently, metal oxide gas sensors (including Cu_2O, In_2O_3, Co_3O_4) have been hybridized with graphene to boost their ability of gas detection at room temperature [53–64].

Zinc oxide (ZnO) is a rising and significant semiconductor due to its large direct band gap of 0.37 eV and large exciton binding energy of 60 mV. ZnO nanoparticles are very popular to use in graphene hybrid systems because it is easy to control their size, morphology, and material properties. We have recently reported decoration of graphene with $Zn_{12}O_{12}$ nanoclusters to open a band gap of 14.5 meV around the Fermi level at K-point [65]. Graphene decorated with ZnO nanoparticles has been proven to heighten the sensitivity towards common toxic gases like CO, NH_3, NO [55], methane [66], NO_2 [67,68], formaldehyde [69,70], H_2 [63], and also to humidity [71].

The objective of this study is employing DFT in order to analyze the electronic and transport properties of the zinc oxide–graphene hybrid nanosensor when in close proximity to the gas molecules such as NH_3, NO, NO_2, H_2O, and H_2S. Variations in the electronic transport properties of the ZnO–graphene sensors are correlated with the sensitivity capability of the device. Our results reveal the promising future of ZnO–graphene hybrid nanostructure in the development of ultra-high sensitive gas sensors.

2. Computational Methods

This paper presents first-principles calculations based on DFT in combination with the non-equilibrium Green's Function (NEGF) method performed in the Atomistix ToolKit (ATK) software package [72–74]. The Perdew, Burke, and Ernzerh (PBE) approach of generalized gradient approximation (GGA) is used for the exchange-correlation function. To expand the electron wave function, a double-ζ polarized basis set is employed. The Grimme van der Waals (vdW) correction (PBE-D2) [75] is utilized in order to take into account the long-range vdW interactions in the adsorption systems [76]. The electronic temperature is kept constant at 300 K, and the plane wave mesh cut-off energy is set to 150 Rydberg.

To mimic a free-standing graphene sheet, we consider a periodic (3 × 10) supercell of graphene in *y* and *z* dimensions. To avoid any image interactions, a vacuum spacing of 15 Å is imposed on the plane in the *x*-direction in which the sheet is not periodic. By employing the conjugate gradient method, the

supercell is allowed to optimize fully until all the final atomic forces are less than 0.01 eV/Å. The first Brillouin zones are sampled using $1 \times 21 \times 11$ k-points in the x, y, and z directions, respectively. In the next step, zinc oxide is placed in the center of the supercell in the vicinity of the C atoms, and then the whole system is optimized again. For the calculations, we increase the k-points to $1 \times 121 \times 111$ in the x, y, and z directions, respectively. The adsorption energy gives us a quantitative explanation of the interaction strength between adsorbent and adsorbate. The adsorption energy of zinc oxide onto the graphene sheet is computed from:

$$E_{ad(ZnO)} = E_{ZnO-Graphene} - E_{Graphene} - E_{ZnO} \tag{1}$$

Here, $E_{ZnO-Graphene}$, $E_{Graphene}$, and E_{ZnO} are the total energies of the ZnO–graphene system, pristine graphene sheet, and the isolated ZnO, respectively. In the last step, the gas molecules including NH_3, NO, NO_2, H_2O, and H_2S are added to the system by placing them in the vicinity of the ZnO. The gas molecule–ZnO–graphene complexes are completely relaxed. The adsorption energies of the gas molecules on the ZnO–graphene system are obtained by:

$$E_{ad(Molecule)} = E_{Molecule-ZnO-Graphene} - E_{ZnO-Graphene} - E_{Molecule} \tag{2}$$

where $E_{Molecule-ZnO-Graphene}$ is the total energy of the molecule–ZnO–graphene compound and $E_{Molecule}$ is the energy of an isolated gas molecule. Mulliken population analysis is engaged to study the charge transfer between the graphene and ZnO and between the gas molecules and the ZnO–graphene system. To simulate the gas sensing system and analyze its electronic and transport properties, the structure is converted to a two-point probe sensor, as shown in Figure 1. The sensor consists of 120 atoms of C which is functionalized with the zinc oxide. It also includes a scattering region (12.8×24.6 Å^2) and 4.92 Å electrodes on each side. It should be noted that the left and right electrodes (the black boxes) are semi-infinite until cells and are repeated along the z-axis. Moreover, the scattering region is periodic along the y-axis. We describe the quantum conductance of the system via the transmission coefficient at the Fermi level:

$$C(E) = G_0 T(E) \tag{3}$$

where $G_0 = 2e^2/h$ is the quantum conductance constant (e is the electron charge and h is Planck's constant). The transmission is calculated along the z-direction. Moreover, transmission coefficients at energy E can be expressed based on the retarded Green's function $G^{\dagger}(E)$ and the advanced Green's functions $G(E)$ of the scattering region.

$$T(E) = G(E)\Gamma^L(E)G^{\dagger}(E)\Gamma^R(E) \tag{4}$$

Here, $\Gamma^{L(R)}(E)$ is the coupling function of the left (right) electrode which is:

$$\Gamma^{L(R)} = \frac{1}{i}\left(\sum{}^{L(R)} - \left(\sum{}^{L(R)}\right)^{\dagger}\right) \tag{5}$$

where $\sum^{L(R)}$ is the electrode self-energy of the left (right) electrode.
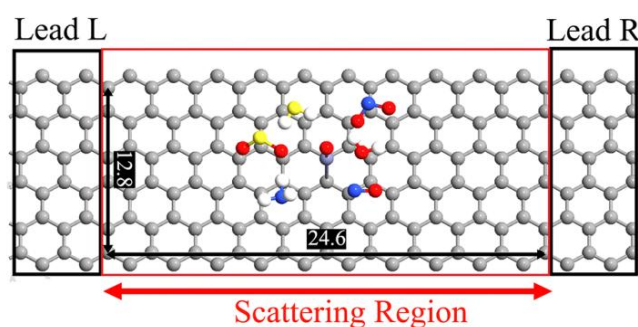
Figure 1. Schematic illustration of zinc oxide (ZnO)–graphene hybrid gas sensor with two leads (black boxes). The gray, purple, red, blue, yellow, and white balls represent C, Zn, O, N, S, and H atoms, respectively. The length and the width of the scattering region (red box) of the sensor (in unit of Å) are also provided.

3. Results and Discussion

We first optimize the ZnO–graphene hybrid nanostructure in order to obtain the most energetically stable geometry of the sensor. ZnO can adhere to the graphene at different positions including the atom site (above C atom), bridge site (above C–C bond), and hollow site (center of C–C hexagons). Additionally, concerning the surface of the graphene sheet, a ZnO can be aligned parallel or upright at these specific positions. The most stable configuration is found by full relaxation of all the possible structures and comparing their final adsorption energies. The most energetically favorable adsorption configuration, which is the arrangement with the minimum adsorption energy, is shown in Figure 2a. Our DFT calculations show that ZnO prefers to place itself perpendicular with respect to the graphene plane, while the Zn atom heading to the C atoms and the O atom way around. The Zn atom is located above the middle of the C_1–C_2 bond and is bonded to C atoms on the graphene sheet to form a Zn–C_1–C_2 triangle with Zn–C_1, Zn–C_2, and C_1–C_2 side lengths of 2.24, 2.20, and 1.44 Å, respectively. The C_1–Zn–C_2 angle is 37.95°. The Zn–O bond length in isolated ZnO (2.00 Å) is reduced to 1.70 Å after interaction with C atoms of the graphene sheet. For ZnO–graphene nanostructure, an adsorption energy of −0.68 eV is obtained that could be indicative of moderate chemisorption. This chemisorption accompanies with an electron transfer of 0.105 *e* from ZnO to graphene. These findings can be confirmed by comparing the band structures of the pristine graphene sheet and the ZnO–graphene hybrid nanostructure, as depicted in Figure 2b. The dashed green curves show the reference results for a pristine graphene sheet. As we know, graphene has no band gap. This means the valence and conduction bands touch at the Dirac points. Upon exposure to zinc oxide, the induced electrons shifted down the Dirac point of the graphene towards negative energies and moved the Fermi level to the conduction band, as shown in Figure 2b in solid black curves. This suggests that the n-type doping effect of graphene has taken place. The Dirac point of the graphene is distorted after interaction with the ZnO due to breakage of bond symmetry in graphene. Interestingly, a gap of 26 meV is observable between the bands *c* (shifted conduction band) and *v* (shifted valence band) of the ZnO–graphene hybrid.

Next, the adsorption mechanisms of the NH_3, NO, NO_2, H_2S, and H_2O gas molecules onto a graphene–ZnO nanostructure sheet are addressed. In the first step, each gas molecule is placed at a distance of 2 Å above the O atom of the ZnO–graphene nanostructure. Some initial configurations are considered. The gas molecules can be aligned in parallel or perpendicular concerning the surface of the ZnO–graphene nanostructure. Further, the N atom of NO with a diatomic molecular structure can point up or down to the ZnO–graphene nanostructure. For the triatomic molecules (NO_2, H_2O, and H_2S) and tetratomic molecule (NH_3), two orientations are examined. In the first orientation, the N atom (in NH_3 and NO_2), O atom (in H_2O), and S atom (in H_2S), point to the O atom of the ZnO–graphene nanostructure, while, in the second one, the O atom (in NO_2) and H atom (in NH_3, H_2O, and H_2S) point down to the surface of the sensor. In the second step, all the input structures are allowed to fully

optimize. Once improved, the structural stability is studied regarding the adsorption energy. The most stable configurations which have the most negative adsorption energies are chosen for further analysis and are depicted in Figure 3. The conventional sensing mechanism is that charge transfer between the adsorbed gas molecules and the surface of the 2D nanomaterials is expected to affect the conductivity of the system upon exposure to the target gas molecules, while the chemical structure of the sensing layer is preserved. The adsorption energies of the gas molecules on the ZnO–graphene nanostructure, the minimum binding distances, and the net charge transfer on molecules using Mulliken population analysis are summarized in Table 1.
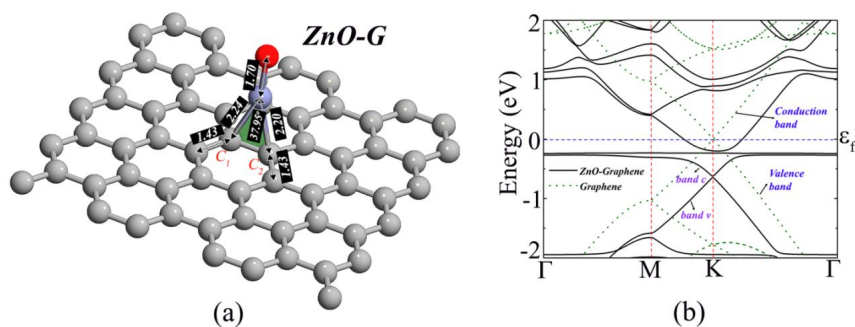
Figure 2. (**a**) Relaxed configuration of the ZnO adsorbed onto a graphene sheet. The gray, purple, and red balls signify C, Zn, and O atoms, respectively. The green area highlights the C_1–Zn–C_2 angle. The bond lengths and the binding distances between the ZnO and the graphene sheet (in unit of Å) are also given. (**b**) The band structures of pristine graphene (dashed green curves) and the ZnO–graphene hybrid (solid black curves).
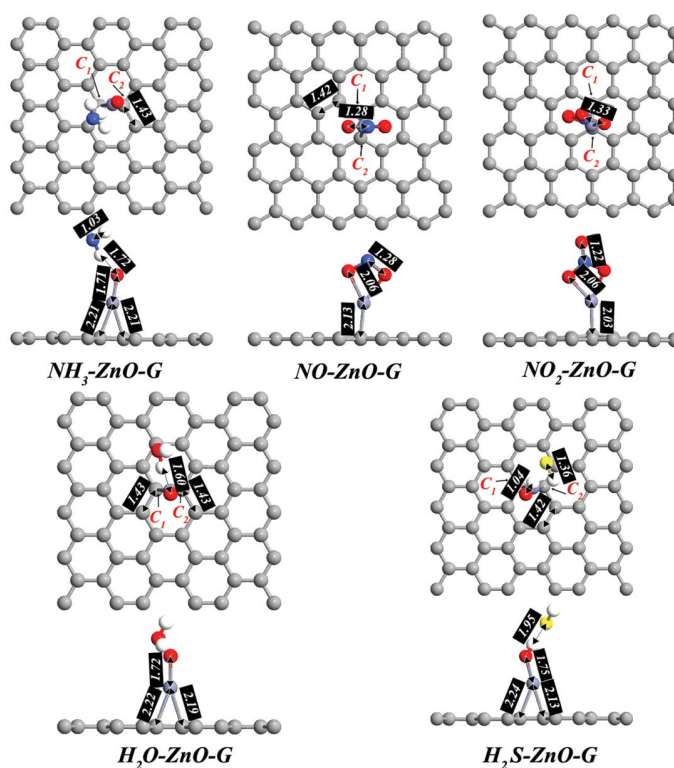
Figure 3. The most stable adsorption configurations (top and side view) for NH_3, NO, NO_2, H_2O, and H_2S on the ZnO–graphene sensor. The gray, purple, red, blue, yellow, and white balls represent C, Zn, O, N, S, and H atoms, respectively. The bond lengths (in unit of Å) and the binding distances between the molecule and the sensor are also provided.

Table 1. The calculated adsorption energy (E_{ad}), binding distance (D) which is the shortest atom to atom distance between the molecule and the sensor, the charge transfer (Q), and the evaluated value of the sensitivity of the sensor with respect to each gas molecule (S). The positive value of charge indicates a charge transfer from the molecule to the sensor.

System	E_{ad} (eV)	D (Å)	Q (e)	S (%)
NH_3-ZnO-G	−0.55	1.72	+0.056	11.8
NO-ZnO-G	−2.21	1.28	+0.155	188.2
NO_2-ZnO-G	−1.85	1.33	+0.141	141.1
H_2O-ZnO-G	−0.32	1.60	+0.031	6.4
H_2S-ZnO-G	−1.01	1.04	+0.121	76.47

We first scrutinize the interactions of the NH_3 molecule and the ZnO–graphene compound. As can be seen in Figure 3, H atom of the NH_3 molecule interacts with the O atom of the ZnO–graphene nanostructure. The interaction distance H-O is found to be 1.72 Å which is larger than the sum of the covalent radii of the H and O atoms (0.95 Å) [77]. Furthermore, the adsorption energy is calculated to be −0.55 eV that is large enough to form a hydrogen bond between the NH_3 and the sensor (H–O). A hydrogen bond is a weak interaction whose strength can be placed between the chemical bond and the vdW force [78]. One can say that the NH_3 molecule is only physically adsorbed on the surface while maintaining its molecular form. The C_1–C_2 bond length remains unchanged while both Zn–C_1 and Zn–C_2 bond lengths are slightly altered to 2.21 Å. The C_1–Zn–C_2 angle is reduced from 37.95° to 14.86°. The bond lengths of N–H in an isolated NH_3 (1.03 Å) are found to be the same after adsorption onto the ZnO–graphene. These small variations substantiate that the influence of NH_3 adsorption onto the sensor is trivial. This observation can be further verified by the low amount of charge (0.056 e) that is transferred from the NH_3 to the graphene-based sensor. Excitingly, the calculated adsorption energy for the NH_3–ZnO–graphene complex is greater than that obtained for NH_3 adsorption onto pristine graphene (−0.11 eV) [7] and is less than the ammonia adsorption energy on the ZnO ($10\bar{1}0$) (−1.32 eV) [79], ZnO (0001) (−2.21 eV) [80], and ZnO (6,0) single-walled nanotube (−0.82 eV) [81] surfaces, revealing that hybridization of pristine graphene with ZnO increases its adsorption capability toward NH_3 significantly. This is in accordance with the experimental data. It was reported that sensors based on ZnO-decorated graphene oxide sheets can detect NH_3 for concentrations as low as 1 ppm at room temperature [55].

Next, the interactions of the NO and NO_2 gas molecules with the ZnO–graphene hybrid are inspected. The relaxed structures are provided in Figure 3. The adsorption energies of NO and NO_2 are −1.21 and −1.85 eV, respectively. One can conclude that there exists a strong chemisorption characteristic between NO and NO_2 gas molecules and the sensor. Upon adsorption of NO on the ZnO–graphene compound, the C_1–C_2 bond length is elongated to 1.45 Å, while Zn–C_1 and Zn–C_2 bond lengths are shortened to 2.13 and 2.18 Å, respectively. Additionally, the C_1–Zn–C_2 angle is slightly increased to 39.58°. The N and O atoms of the NO interact with O and Zn atoms of ZnO, respectively, to form a kite where its four sides can be grouped into two pairs of equal-length sides (N–O and Zn–O) that are adjacent to each other. The length of N–O is 1.28 Å and Zn–O equals to 2.06 Å. The N–O bond length is stretched from 1.17 Å in an isolated NO molecule to 1.28 Å in the NO–ZnO–graphene system. The O–N–O and O–Zn–O angles of the kite are 113.10° and 92.46°, respectively. The interaction of NO_2 and ZnO–graphene bears many similarities to that of the NO and ZnO–graphene. In much the same manner, the interaction between the NO part of the NO_2 molecule and ZnO results in the Zn–O–N–O kite. In this geometry, the lengths of the N–O sides equal to 1.33 Å and the Zn–O sides have the length of 2.06 Å. The O–N–O and O–Zn–O angles of the kite are 113.92° and 91.16°, respectively. In comparison with the length of N–O bonds in the isolated NO_2 (1.21 Å), the N–O bond of the NO_2 in the kite gets extended to 1.33 Å, while the second N–O bond of the molecule remains almost unchanged. It should be added that the O–N–O bond angle of isolated NO_2 decreases from 133.06° to 122.38° after complexation with ZnO–graphene compound. Despite the resemblances above between NO and NO_2

adsorption on the ZnO–graphene sensor, the Zn atom is shifted from above the middle of C_1–C_2 bond to top of the C_2 atom, where both Zn–C_1 and Zn–C_2 bond lengths are 2.50 and 2.03 Å, respectively. Interestingly, after exposure to NO_2, the C_1–C_2 bond length is stretched to 1.46 Å. Additionally, the C_2 atom protrudes outwards after NO_2 adsorption with a buckling distance of ~0.302 Å. These noticeable changes in the structure of the ZnO–graphene sensor are indicative of the chemical adsorption of NO and NO_2 and agree well with the calculated adsorption energies for the gas molecules on the sensor. The obtained adsorption energies for NO (−1.21 eV) and NO_2 (−1.85 eV) on the ZnO–graphene are considerably higher compared to those reported for NO (−0.30 eV) and NO_2 (−0.48 eV) adsorption onto pristine graphene [7] and those obtained for NO (−0.28 eV) and NO_2 (−0.36 eV) adsorption onto the ZnO $(10\bar{1}0)$ surface [82] and for NO (−0.40 eV) and NO_2 (−0.31 eV) adsorption onto the ZnO $(2\bar{1}\bar{1}0)$ surface [83]. It should be noted that the gas adsorption does not change the chemical structure of the sensing layer. As mentioned earlier, the sensing mechanism of the gas molecules is due to the charge transfer between the target gas molecules and the sensing layer. A significant amount of charge transfer is observed from NO (0.155 e) and NO_2 (0.141 e) to the sensor. The large electron transfer in these systems can be attributed to the strong chemisorption of the NO and NO_2 gas molecules on the sensor. Such a large charge transfer is expected to induce considerable changes in the conductivity of the system which will be discussed later. The experimental data support our theoretical findings. Singh et al. discovered that ZnO decorated graphene sheet sensor responses to 5 ppm NO gas in dry nitrogen at room temperature [55]. Furthermore, Liu et al. reported that the introduction of ZnO nanoparticles into reduced graphene oxide matrix enhances its sensing performance for NO_2 at room temperature [67].

　　We also evaluate the sensitivity of the ZnO–graphene sensor to the H_2O and H_2S gas molecules. Figure 3 depicts the most stable configuration of the H_2O and H_2S–ZnO–graphene complexes. For H_2O, our computational results indicate that it is weakly physisorbed on the sensor with an adsorption energy of −0.32 eV which is higher than its adsorption energy on pristine graphene (−0.027 eV) [84] and the pristine ZnO (0001) surface (−0.28 eV) [85], while it is less than its adsorption energy on the pristine ZnO $(10\bar{1}0)$ surface (−0.94 eV) [86]. Hence, the ZnO–graphene sensor demonstrates promise to work under humid air. A charge of 0.031 e is transferred from the water molecule to the sensor. The minimum distance between the H_2O and the sensor is 1.60 Å and this occurred between H of the H_2O and O of the ZnO which is larger than the sum of the covalent radii of the H and O atoms (0.95 Å) [77]. One can conclude that there exists a weak hydrogen-bonding interaction between H_2O and the sensor. Therefore, the sensor undergoes minor structural changes when is exposed to H_2O (also known as, humidity). Consequently, H_2O is only physisorbed on the surface while preserving its molecular form. The Zn–C_1 and Zn–C_2 are slightly reduced to 2.22 and 2.19 Å, respectively, while C_1–C_2 is kept unchanged. The C_1–Zn–C_2 angle is increased to 38.22°, and the Zn–O bond length is extended to 1.72 Å. These small variations in the sensor are in agreement with the results obtained for the adsorption energy and charge transfer, and confirm the weak physisorption of the water molecule by the sensor. The H_2S adsorption mechanism on ZnO–graphene is more complicated than the other molecules studied above. The H_2S molecule and the sensor experience substantial structural changes after adsorption process. The H–S bond lengths in isolated H_2S (1.35 Å) are extended to 1.36 and 1.95 Å, indicating that the molecule is fully dissociated during the adsorption process into the chemisorbed H and separated HS species. While the first HS bond dissociates, the second one does not. Therefore, dissociation of adsorbed H_2S to adsorbed H and HS occurs on the surface of ZnO according to the following process:

$$H_2S_{(ada)} \rightarrow HS + H_{(ads)} \tag{6}$$

　　The H atom of the molecule forms a covalent bond with the O atom of the ZnO with a bond length of 1.75 Å. The H–S–H bond angle of the isolated H_2S increases from 91.29° to 92.63° after complexation with ZnO-graphene sensor. The Zn–C_1, Zn–C_2, and C_1–C_2 bond lengths are 2.24, 2.13, and 1.45 Å, respectively. Although H_2S and H_2O are quite similar molecules, the strength of the HS compared to HO bonds is significantly different. The much higher preference of H_2S

to dissociate in comparison with H_2O can be related to the different acidity of the two molecules and the much lower pKa value of H_2S [87]. The adsorption energy of H_2S on the ZnO–graphene compound is -1.01 eV which is accompanied by a charge transfer of 0.121 e from the molecule to the sensor. H_2S prefers to dissociatively adsorb on the ZnO $(10\bar{1}0)$ surface with an adsorption energy of -1.36 eV [88]. Moreover, the calculated E_{ad} of H_2S on the ZnO–graphene compound is higher than the values reported for its adsorption on the pristine graphene (-0.11 eV) [89], pristine ZnO (0001) (-0.91 eV) [90], and pristine hexagonal monolayer ZnO (-0.54 eV) [91] surfaces, proposing the great capability of the ZnO–graphene hybrid for H_2S dissociation. The experimental reported data confirm our DFT findings. Song et al. experimentally shown that the dispersion of ZnO nanoparticle on the reduced graphene sheet promotes the H_2S adsorption capacities [92]. Moreover, Cuong et al. demonstrated that a sensor based on vertically aligned ZnO nanorods on a graphene film effectively detects 2 ppm of H_2S in oxygen at room temperature [93].

In order to better understand the binding strength of the gas molecules adsorption, the electronic total charges density of ZnO–graphene is obtained and compared with those calculated for gas molecules–ZnO–graphene complexes, as shown in Figure 4. An orbital overlap can be observed between ZnO and the graphene sheet, confirming this theory that ZnO is chemically adsorbed on the graphene sheet. For NO and NO_2, an orbital overlap can be seen between the gas molecules and the ZnO, revealing the occurrence of the strong chemisorption. This strong orbital mixing is attributed to the large charge transfer to the sensor. The weak interactions of the NH_3 and H_2O with the ZnO–graphene sensor can be verified by studying the electronic total charge densities of the molecules-sensor compound. It can be seen that there is no orbital overlap between the molecules previously stated and the sensor. In consistent with our obtained results, while the electron density of the H atom of the H_2S is bonded with the O atom of the ZnO, the HS part of the gas molecule has no overlap with the sensor, confirming the full dissociation of the hydrogen sulfide molecule through the adsorption process.
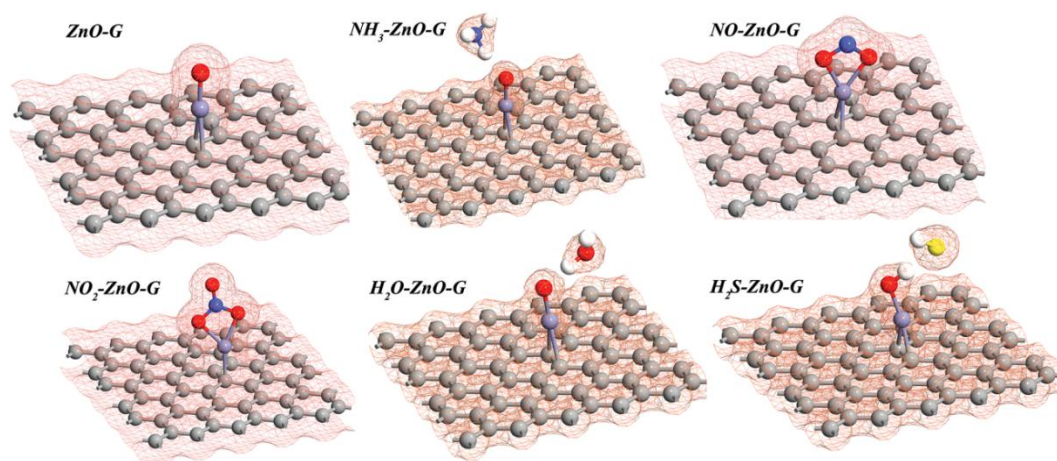

Figure 4. The electronic total charge densities of the ZnO–graphene sensor before and after complexation with NH_3, NO, NO_2, H_2O, and H_2S. The gray, purple, red, blue, yellow, and white balls represent C, Zn, O, N, S, and H atoms, respectively.

It is worth mentioning that the electronic properties of the sensor undergo significant changes owing to orbital mixing and the charge transfer between the molecule and the sensor, which is favorable for gas sensing applications. To explore the effect of gas molecules adsorption on the electronic properties of the sensor, the band structure of the ZnO–graphene sensor before and after exposure are calculated, and plotted in Figure 5. As discussed earlier, the ZnO–graphene sensor shows n-type behavior due to the transferred electrons from the ZnO to graphene. This causes a downward shift of the graphene's Dirac point to the negative energies and opens a gap of 26 meV

between conduction (band c) and valence (band v) bands of the graphene, which are highlighted with green color in Figure 5. When the ZnO–graphene sensor is exposed to the gas molecules, different amount of electrons are transferred from the molecules to the sensor which dropped more the K-point of the hybrid structure. The band structure of the sensor changed a little upon adsorption of NH_3 and H_2O. However, the variation in the electronic properties of the sensor after NH_3 adsorption (mostly in the c band) is more pronounced compared to that upon H_2O adsorption. The gap of the hybrid sensor is slightly increased to 33 and 30 meV after NH_3 and H_2O adsorption. These small changes agree well with the small number of electrons transferred from NH_3 (+0.056 e) and H_2O (+0.031 e) to the sensor. Upon exposure to NO and NO_2, the c and v bands are shifted even more to the negative energies, implying that the sensor's n-type behavior is enhanced. The reason for this phenomena is the large electron transfer after adsorption of NO (+0.155 e) and NO_2 (+0.141 e) onto the sensor. Additionally, the gap between the bands are widened to 68 and 171 meV after the interaction of the sensor with NO and NO_2 gas molecules, correspondingly. Finally, the band structure of the sensor undergoes substantial alterations after interacting with the H_2S gas molecule. The energy range of band c is extended towards the positive electron energies, while the energy range of band v is shrunken. Moreover, the gap between bands c and v at K-point increases to 66 meV, while its location is moved down. These changes can be attributed to the dissociation of the H_2S after interacting with the sensor inducing an electron transfer of +0.121 e from the molecule to the sensor.
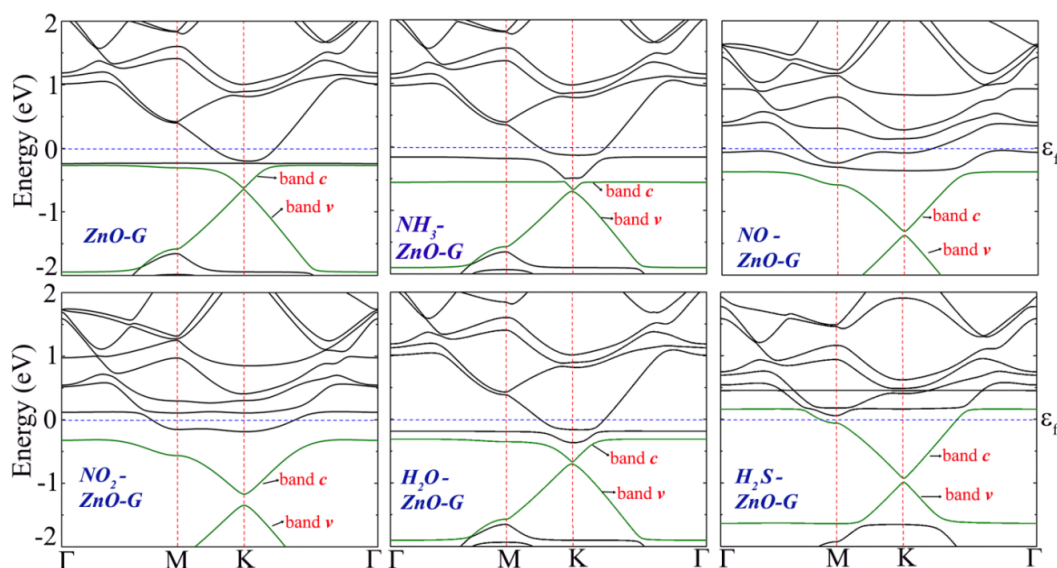
Figure 5. The electronic band structures of the ZnO–graphene sensor before and after adsorption of NH_3, NO, NO_2, H_2O, and H_2S. Valance and conduction bands are highlighted in green. The Fermi levels, indicated in blue dashed lines, have been set to 0 eV.

The charge transfer caused by the gas molecules adsorption brings about alterations in the conductance of the sensor which is a key element for assessing the performance of the substrate material. To learn about the impacts of the gas molecule adsorption on the transport properties of the sensor, we calculate the quantum conductances of the two-point probe sensor (see Figure 1) with and without the gas molecules' adsorption, as plotted in Figure 6. This also helps us understand better the ability of the sensor to detect the aforementioned gas molecules. As seen in Figure 6, pristine graphene shows semi-metallic behavior with zero band gap and zero conductance at the Fermi level. The ZnO adsorption significantly stimulates the transport property of graphene. The electronic states of the ZnO–graphene hybrid at the Fermi level are noticeably increased due to the electrons transfer, resulting in an enhancement to the conductance of the system. The quantum conductance of the sensor is found to be 0.34 $2e^2/h$ at the Fermi level. In addition, the metallic ZnO–graphene compound shows

a peak at electron energy of -0.24 eV. The conductance of the compound drops to zero at electron energy of -0.64 eV, confirming the existence of a gap between c and v bands in its band structure, as discussed before. The conductances of the ZnO–graphene sensor before and after adsorption of NH_3 and H_2O molecules vary very little, suggesting low level of sensitivity to these molecules. However, the alterations of the quantum conductances are more prominent for the other complexes. Once NO (NO_2) is absorbed on the sensor, the quantum conductance of the sensor increases from 0.34 to 0.97 (0.81) $2e^2/h$. Furthermore, the sensor shows no conductivity for the electron energy range of -1.28 to -1.11 eV after NO_2 adsorption and -1.40 to -1.33 eV after interaction with NO, which concurs well with our previous findings for their corresponding band structures. The observable conductance changes, high adsorption energy, and large charge transfer indicate the promising applications of the ZnO–graphene as a sensitive chemical sensor for NO and NO_2 detection. One can also see that the interactions of the H_2S with the sensor increase the quantum conductance to 0.59 $2e^2/h$. The quantum conductance of the sensor after adsorption of H_2S is zero in the electron energy between -1.02 to -0.95 eV, indicating a shift of 0.36 eV to the negative electron energies in comparison with that of an unexposed sensor. Consequently, the ZnO–graphene sensor might be a potential catalyst for dissociation of the H_2S gas molecule. These results are in good agreement with reported experimental results, showing that the ability of graphene-based sensors to detect NH_3 [55], NO [55], NO_2 [67,94], and H_2S [57,95] are significantly enhanced after adsorption of ZnO.
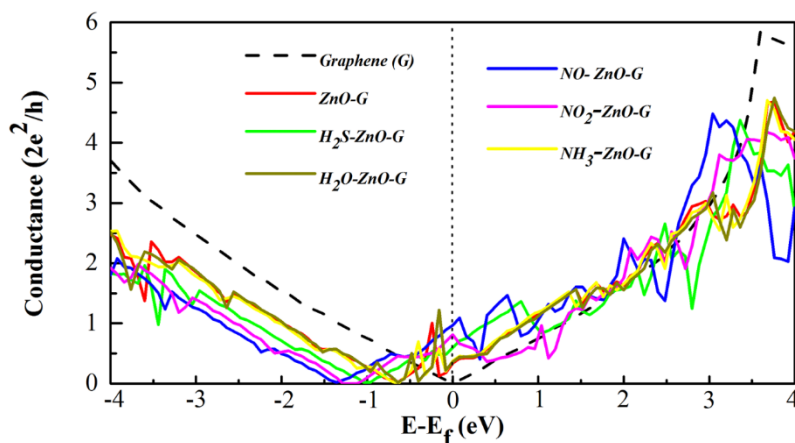
Figure 6. Quantum conductance of the ZnO–graphene sensor before and after complexation with NH_3, NO, NO_2, H_2O, and H_2S as a function of electron energy.

The sensing capability of the ZnO–graphene sensor to various gas molecules are also assessed by quantifying its sensitivity, which can be expressed as follows:

$$S(\%) = \frac{|C - C_0|}{C_0} \tag{7}$$

Here, C and C_0 are the zero bias conductances for the nanosensor with and without the gas molecules, respectively. The results obtained are listed in Table 1. The sensitivities of NH_3, NO, NO_2, H_2O, and H_2S gas molecules on the sensor are calculated to be 11.8%, 188.2%, 141.1%, 6.4%, and 76.47%, respectively. The sensitivities of the sensor to NO, NO_2, and H_2S are much larger than its sensitivity to H_2O, showing superior sensitivity and selectivity toward those gas molecules even in the presence of water vapor. Another important factor for evaluating the performance of a gas sensor is the recovery time (τ), which can be described using conventional transition state theory as follows:

$$\tau \propto \exp(-E_{ad}/k_B T) \tag{8}$$

A small adsorption energy can result in a fast desorption process of the gases from the sensor. The recovery time is found to follow an ascending order of $H_2O < NH_3 < H_2S < NO_2 < NO$. The sensor shows a low level of sensitivity to the NH_3 in spite of the short recovery time. Interestingly, the sensor shows promise to work under humid air as a result of its low sensitivity and quick recovery time to water molecules. Since the chemisorption of NO_2 and NO is accompanied with high adsorption energies, much longer time is necessary to completely desorb the gas molecules. Hence, the ZnO–graphene sensor can be utilized as a disposable molecule sensor for specific NO and NO_2 detection. Lastly, the moderate adsorption energy for H_2S suggests that it is possible to desorb it from the sensor by heating at room temperature, revealing a great potential of the ZnO–graphene hybrid to be used as H_2S catalyst.

4. Conclusions

We performed detailed first-principles computational analysis on the geometric and electronic transport properties of the ZnO–graphene hybrid gas sensor upon interaction with NH_3, NO, NO_2, H_2O, and H_2S gas molecules. It was found that NH_3 and H_2O are adsorbed on the sensor with weak hydrogen bonds. These weak interactions caused small variations in the electronic transport properties of the sensor that can be attributed to the small charge transfer from NH_3 and H_2O to the sensor. However, the NO and NO_2 are chemisorbed with a high adsorption energy and large charge transfer, resulting in significant alterations in the conductance of the ZnO–graphene hybrid gas sensor. Interestingly, the H_2S gas molecule is chemisorbed through a dissociative mechanism which is accompanied by a large charge transfer from the molecule to the sensor, leaving noticeable changes in the electronic transport properties of the sensor. Consequently, ZnO–graphene is a potential material for NO and NO_2 detection and is a propitious catalyst for H_2S dissociation.

Author Contributions: S.B. and C.W. conceived the original idea; I.T., S.M.A. and A.R.B. performed the simulations; I.T. and S.M.A. analyzed the results; I.T. and S.M.A. wrote the paper.

References

1. Novoselov, K.S.; Geim, A.K.; Morozov, S.V.; Jiang, D.; Zhang, Y.; Dubonos, S.V.; Grigorieva, I.V.; Firsov, A.A. Electric field effect in atomically thin carbon films. *Science* **2004**, *306*, 666–669. [CrossRef] [PubMed]

2. Novoselov, K.S.; Geim, A.K.; Morozov, S.; Jiang, D.; Katsnelson, M.; Grigorieva, I.; Dubonos, S.; Firsov, A. Two-dimensional gas of massless Dirac fermions in graphene. *Nature* **2005**, *438*, 197–200. [CrossRef] [PubMed]

3. Schedin, F.; Geim, A.; Morozov, S.; Hill, E.; Blake, P.; Katsnelson, M.; Novoselov, K. Detection of individual gas molecules adsorbed on graphene. *Nat. Mater.* **2007**, *6*, 652–655. [CrossRef] [PubMed]

4. Basu, S.; Bhattacharyya, P. Recent developments on graphene and graphene oxide based solid state gas sensors. *Sens. Actuators B Chem.* **2012**, *173*, 1–21. [CrossRef]

5. He, Q.; Wu, S.; Yin, Z.; Zhang, H. Graphene-based electronic sensors. *Chem. Sci.* **2012**, *3*, 1764–1772. [CrossRef]

6. Leenaerts, O.; Partoens, B.; Peeters, F. Adsorption of H_2O, NH_3, CO, NO_2, and NO on graphene: A first-principles study. *Phys. Rev. B* **2008**, *77*, 125416. [CrossRef]

7. Zhang, Y.-H.; Chen, Y.-B.; Zhou, K.-G.; Liu, C.-H.; Zeng, J.; Zhang, H.-L.; Peng, Y. Improving gas sensing properties of graphene by introducing dopants and defects: A first-principles study. *Nanotechnology* **2009**, *20*, 185504. [CrossRef] [PubMed]

8. Dai, J.; Yuan, J.; Giannozzi, P. Gas adsorption on graphene doped with B, N, Al, and S: A theoretical study. *Appl. Phys. Lett.* **2009**, *95*, 232105. [CrossRef]

9. Robinson, J.T.; Perkins, F.K.; Snow, E.S.; Wei, Z.; Sheehan, P.E. Reduced graphene oxide molecular sensors. *Nano Lett.* **2008**, *8*, 3137–3140. [CrossRef] [PubMed]

10. Lu, G.; Ocola, L.E.; Chen, J. Reduced graphene oxide for room-temperature gas sensors. *Nanotechnology* **2009**, *20*, 445502. [CrossRef] [PubMed]

11. Dai, J.; Yuan, J. Adsorption of molecular oxygen on doped graphene: Atomic, electronic, and magnetic properties. *Phys. Rev. B* **2010**, *81*, 165414. [CrossRef]

12. Nasehnia, F.; Seifi, M. Adsorption of molecular oxygen on VIIIB transition metal-doped graphene: A DFT study. *Mod. Phys. Lett. B* **2014**, *28*, 1450237. [CrossRef]

13. Borisova, D.; Antonov, V.; Proykova, A. Hydrogen sulfide adsorption on a defective graphene. *Int. J. Quantum Chem.* **2013**, *113*, 786–791. [CrossRef]

14. Liu, W.; Liu, Y.; Wang, R.; Hao, L.; Song, D.; Li, Z. DFT study of hydrogen adsorption on Eu-decorated single-and double-sided graphene. *Phys. Status Solidi B* **2014**, *251*, 229–234. [CrossRef]

15. Fowler, J.D.; Allen, M.J.; Tung, V.C.; Yang, Y.; Kaner, R.B.; Weiller, B.H. Practical chemical sensors from chemically derived graphene. *ACS Nano* **2009**, *3*, 301–306. [CrossRef] [PubMed]

16. Ko, G.; Kim, H.-Y.; Ahn, J.; Park, Y.-M.; Lee, K.-Y.; Kim, J. Graphene-based nitrogen dioxide gas sensors. *Curr. Appl. Phys.* **2010**, *10*, 1002–1004. [CrossRef]

17. Chen, G.; Paronyan, T.M.; Harutyunyan, A.R. Sub-ppt gas detection with pristine graphene. *Appl. Phys. Lett.* **2012**, *101*, 053119. [CrossRef]

18. Some, S.; Xu, Y.; Kim, Y.; Yoon, Y.; Qin, H.; Kulkarni, A.; Kim, T.; Lee, H. Highly sensitive and selective gas sensor using hydrophilic and hydrophobic graphenes. *Sci. Rep.* **2013**, *3*, 1868. [CrossRef] [PubMed]

19. Fattah, A.; Khatami, S. Selective H_2S Gas Sensing with a Graphene/n-Si Schottky Diode. *IEEE Sens. J.* **2014**, *14*, 4104–4108. [CrossRef]

20. Prezioso, S.; Perrozzi, F.; Giancaterini, L.; Cantalini, C.; Treossi, E.; Palermo, V.; Nardone, M.; Santucci, S.; Ottaviano, L. Graphene oxide as a practical solution to high sensitivity gas sensing. *J. Phys. Chem. C* **2013**, *117*, 10683–10690. [CrossRef]

21. Hafiz, S.M.; Ritikos, R.; Whitcher, T.J.; Razib, N.M.; Bien, D.C.S.; Chanlek, N.; Nakajima, H.; Saisopa, T.; Songsiriritthigul, P.; Huang, N.M. A practical carbon dioxide gas sensor using room-temperature hydrogen plasma reduced graphene oxide. *Sens. Actuators B Chem.* **2014**, *193*, 692–700. [CrossRef]

22. Hu, N.; Wang, Y.; Chai, J.; Gao, R.; Yang, Z.; Kong, E.S.-W.; Zhang, Y. Gas sensor based on p-phenylenediamine reduced graphene oxide. *Sens. Actuators B Chem.* **2012**, *163*, 107–114. [CrossRef]

23. Kwon, Y.J.; Cho, H.Y.; Na, H.G.; Lee, B.C.; Kim, S.S.; Kim, H.W. Improvement of gas sensing behavior in reduced graphene oxides by electron-beam irradiation. *Sens. Actuators B Chem.* **2014**, *203*, 143–149. [CrossRef]

24. Topsakal, M.; Aktürk, E.; Sevinçli, H.; Ciraci, S. First-principles approach to monitoring the band gap and magnetic state of a graphene nanoribbon via its vacancies. *Phys. Rev. B* **2008**, *78*, 235435. [CrossRef]

25. Lu, P.; Zhang, Z.; Guo, W. Electronic and magnetic properties of zigzag edge graphene nanoribbons with Stone–Wales defects. *Phys. Lett. A* **2009**, *373*, 3354–3358. [CrossRef]

26. Lopez-Bezanilla, A.; Zhou, W.; Idrobo, J.-C. Electronic and Quantum Transport Properties of Atomically Identified Si Point Defects in Graphene. *J. Phys. Chem. Lett.* **2014**, *5*, 1711–1718. [CrossRef] [PubMed]

27. Aghaei, S.M.; Monshi, M.M.; Torres, I.; Calizo, I. Edge functionalization and doping effects on the stability, electronic and magnetic properties of silicene nanoribbons. *RSC Adv.* **2016**, *6*, 17046–17058. [CrossRef]

28. Rad, A.S. First principles study of Al-doped graphene as nanostructure adsorbent for NO_2 and N_2O: DFT calculations. *Appl. Surf. Sci.* **2015**, *357*, 1217–1224. [CrossRef]

29. Tit, N.; Said, K.; Mahmoud, N.M.; Kouser, S.; Yamani, Z.H. Ab-initio investigation of adsorption of CO and CO_2 molecules on graphene: Role of intrinsic defects on gas sensing. *Appl. Surf. Sci.* **2017**, *394*, 219–230. [CrossRef]

30. Ma, L.; Zhang, J.-M.; Xu, K.-W.; Ji, V. A first-principles study on gas sensing properties of graphene and Pd-doped graphene. *Appl. Surf. Sci.* **2015**, *343*, 121–127. [CrossRef]

31. Gupta, S.; Sabarou, H.; Zhong, Y.; Singh, P. Phase evolution and electrochemical performance of iron doped lanthanum strontium chromite in oxidizing and reducing atmosphere. *Int. J. Hydrogen Energy* **2017**, *42*, 6262–6271. [CrossRef]

32. Chawla, N.; Chamaani, A.; Safa, M.; El-Zahab, B. Palladium-Filled Carbon Nanotubes Cathode for Improved Electrolyte Stability and Cyclability Performance of $Li-O_2$ Batteries. *J. Electrochem. Soc.* **2017**, *164*, A6303–A6307. [CrossRef]

33.　Basu, S.; Hazra, S.K. Graphene–Noble Metal Nano-Composites and Applications for Hydrogen Sensors. *C* **2017**, *3*, 29. [CrossRef]

34.　Li, H.; Yin, Z.; He, Q.; Li, H.; Huang, X.; Lu, G.; Fam, D.W.H.; Tok, A.I.Y.; Zhang, Q.; Zhang, H. Fabrication of single-and multilayer MoS_2 film-based field-effect transistors for sensing NO at room temperature. *Small* **2012**, *8*, 63–67. [CrossRef] [PubMed]

35.　He, Q.; Zeng, Z.; Yin, Z.; Li, H.; Wu, S.; Huang, X.; Zhang, H. Fabrication of Flexible MoS_2 Thin-Film Transistor Arrays for Practical Gas-Sensing Applications. *Small* **2012**, *8*, 2994–2999. [CrossRef] [PubMed]

36.　Donarelli, M.; Prezioso, S.; Perrozzi, F.; Bisti, F.; Nardone, M.; Giancaterini, L.; Cantalini, C.; Ottaviano, L. Response to NO_2 and other gases of resistive chemically exfoliated MoS_2-based gas sensors. *Sens. Actuators B Chem.* **2015**, *207*, 602–613. [CrossRef]

37.　Kou, L.; Frauenheim, T.; Chen, C. Phosphorene as a superior gas sensor: Selective adsorption and distinct IV response. *J. Phys. Chem. Lett.* **2014**, *5*, 2675–2681. [CrossRef] [PubMed]

38.　Abbas, A.N.; Liu, B.; Chen, L.; Ma, Y.; Cong, S.; Aroonyadet, N.; Köpf, M.; Nilges, T.; Zhou, C. Black phosphorus gas sensors. *ACS Nano* **2015**, *9*, 5618–5624. [CrossRef] [PubMed]

39.　Mahabal, M.S.; Deshpande, M.D.; Hussain, T.; Ahuja, R. Sensing Characteristics of a Graphene-like Boron Carbide Monolayer towards Selected Toxic Gases. *Chemphyschem* **2015**, *16*, 3511–3517. [CrossRef] [PubMed]

40.　Aghaei, S.M.; Monshi, M.; Torres, I.; Zeidi, S.; Calizo, I. DFT study of adsorption behavior of NO, CO, NO_2, and NH_3 molecules on graphene-like BC_3: A search for highly sensitive molecular sensor. *Appl. Surf. Sci.* **2018**, *427*, 326–333. [CrossRef]

41.　Huo, N.; Yang, S.; Wei, Z.; Li, S.-S.; Xia, J.-B.; Li, J. Photoresponsive and gas sensing field-effect transistors based on multilayer WS_2 nanoflakes. *Sci. Rep.* **2014**, *4*, 5209. [CrossRef] [PubMed]

42.　O'Brien, M.; Lee, K.; Morrish, R.; Berner, N.C.; McEvoy, N.; Wolden, C.A.; Duesberg, G.S. Plasma assisted synthesis of WS_2 for gas sensing applications. *Chem. Phys. Lett.* **2014**, *615*, 6–10. [CrossRef]

43.　Hu, W.; Xia, N.; Wu, X.; Li, Z.; Yang, J. Silicene as a highly sensitive molecule sensor for NH_3, NO and NO_2. *Phys. Chem. Chem. Phys.* **2014**, *16*, 6957–6962. [CrossRef] [PubMed]

44.　Chandiramouli, R.; Srivastava, A.; Nagarajan, V. NO adsorption studies on silicene nanosheet: DFT investigation. *Appl. Surf. Sci.* **2015**, *351*, 662–672. [CrossRef]

45.　Aghaei, S.M.; Monshi, M.M.; Calizo, I. A theoretical study of gas adsorption on silicene nanoribbons and its application in a highly sensitive molecule sensor. *RSC Adv.* **2016**, *6*, 94417–94428. [CrossRef]

46.　Monshi, M.M.; Aghaei, S.M.; Calizo, I. Doping and defect-induced germanene: A superior media for sensing H_2S, SO_2, and CO_2 gas molecules. *Surf. Sci.* **2017**, *665*, 96–102. [CrossRef]

47.　Rai, P.; Kwak, W.-K.; Yu, Y.-T. Solvothermal synthesis of ZnO nanostructures and their morphology-dependent gas-sensing properties. *ACS Appl. Mater. Interfaces* **2013**, *5*, 3026–3032. [CrossRef] [PubMed]

48.　Maeng, S.; Kim, S.-W.; Lee, D.-H.; Moon, S.-E.; Kim, K.-C.; Maiti, A. SnO_2 nanoslab as NO_2 sensor: Identification of the NO_2 sensing mechanism on a SnO_2 surface. *ACS Appl. Mater. Interfaces* **2013**, *6*, 357–363. [CrossRef] [PubMed]

49.　Chen, M.; Wang, Z.; Han, D.; Gu, F.; Guo, G. Porous ZnO polygonal nanoflakes: Synthesis, use in high-sensitivity NO_2 gas sensor, and proposed mechanism of gas sensing. *J. Phys. Chem. C* **2011**, *115*, 12763–12773. [CrossRef]

50.　Rossinyol, E.; Prim, A.; Pellicer, E.; Arbiol, J.; Hernández-Ramírez, F.; Peiró, F.; Cornet, A.; Morante, J.R.; Solovyov, L.A.; Tian, B. Synthesis and Characterization of Chromium-Doped Mesoporous Tungsten Oxide for Gas Sensing Applications. *Adv. Funct. Mater.* **2007**, *17*, 1801–1806. [CrossRef]

51.　Epifani, M.; Díaz, R.; Arbiol, J.; Comini, E.; Sergent, N.; Pagnier, T.; Siciliano, P.; Faglia, G.; Morante, J.R. Nanocrystalline Metal Oxides from the Injection of Metal Oxide Sols in Coordinating Solutions: Synthesis, Characterization, Thermal Stabilization, Device Processing, and Gas-Sensing Properties. *Adv. Funct. Mater.* **2006**, *16*, 1488–1498. [CrossRef]

52.　Hazra, S.K.; Basu, S. Graphene-Oxide Nano Composites for Chemical Sensor Applications. *C* **2016**, *2*, 12. [CrossRef]

53.　Lin, Q.; Li, Y.; Yang, M. Tin oxide/graphene composite fabricated via a hydrothermal method for gas sensors working at room temperature. *Sens. Actuators B Chem.* **2012**, *173*, 139–147. [CrossRef]

54.　Zhang, H.; Feng, J.; Fei, T.; Liu, S.; Zhang, T. SnO_2 nanoparticles-reduced graphene oxide nanocomposites for NO_2 sensing at low operating temperature. *Sens. Actuators B Chem.* **2014**, *190*, 472–478. [CrossRef]

55. Singh, G.; Choudhary, A.; Haranath, D.; Joshi, A.G.; Singh, N.; Singh, S.; Pasricha, R. ZnO decorated luminescent graphene as a potential gas sensor at room temperature. *Carbon* **2012**, *50*, 385–394. [CrossRef]

56. Jammula, R.K.; Srikanth, V.V.; Hazra, B.K.; Srinath, S. ZnO nanoparticles' decorated reduced-graphene oxide: Easy synthesis, unique polarization behavior, and ionic conductivity. *Mater. Des.* **2016**, *110*, 311–316. [CrossRef]

57. Lonkar, S.P.; Pillai, V.; Abdala, A.; Mittal, V. In situ formed graphene/ZnO nanostructured composites for low temperature hydrogen sulfide removal from natural gas. *RSC Adv.* **2016**, *6*, 81142–81150. [CrossRef]

58. Zhou, L.; Shen, F.; Tian, X.; Wang, D.; Zhang, T.; Chen, W. Stable Cu_2O nanocrystals grown on functionalized graphene sheets and room temperature H_2S gas sensing with ultrahigh sensitivity. *Nanoscale* **2013**, *5*, 1564–1569. [CrossRef] [PubMed]

59. Mohammadi-Manesh, E.; Vaezzadeh, M.; Saeidi, M. Theoretical study on electronic structure, and electrical conductance at room temperature of Cu_2O–GS nanosensors and detection of H_2S gas. *Comput. Mater. Sci.* **2015**, *97*, 181–185. [CrossRef]

60. Fu, D.; Han, G.; Chang, Y.; Dong, J. The synthesis and properties of ZnO–graphene nano hybrid for photodegradation of organic pollutant in water. *Mater. Chem. Phys.* **2012**, *132*, 673–681. [CrossRef]

61. Shi, J.; Cheng, Z.; Gao, L.; Zhang, Y.; Xu, J.; Zhao, H. Facile synthesis of reduced graphene oxide/hexagonal WO_3 nanosheets composites with enhanced H_2S sensing properties. *Sens. Actuators B Chem.* **2016**, *230*, 736–745. [CrossRef]

62. Chen, N.; Li, X.; Wang, X.; Yu, J.; Wang, J.; Tang, Z.; Akbar, S. Enhanced room temperature sensing of Co_3O_4-intercalated reduced graphene oxide based gas sensors. *Sens. Actuators B Chem.* **2013**, *188*, 902–908. [CrossRef]

63. Anand, K.; Singh, O.; Singh, M.P.; Kaur, J.; Singh, R.C. Hydrogen sensor based on graphene/ZnO nanocomposite. *Sens. Actuators B Chem.* **2014**, *195*, 409–415. [CrossRef]

64. Khadem, S.J.; Abdi, Y.; Darbari, S.; Ostovari, F. Investigating the effect of gas absorption on the electromechanical and electrochemical behavior of graphene/ZnO structure, suitable for highly selective and sensitive gas sensors. *Curr. Appl. Phys.* **2014**, *14*, 1498–1503. [CrossRef]

65. Monshi, M.M.; Aghaei, S.M.; Calizo, I. Band gap opening and optical absorption enhancement in graphene using ZnO nanocluster. *Phys. Lett. A* **2018**, *382*, 1171–1175. [CrossRef]

66. Zhang, D.; Yin, N.; Xia, B. Facile fabrication of ZnO nanocrystalline-modified graphene hybrid nanocomposite toward methane gas sensing application. *J. Mater. Sci. Mater. Electron.* **2015**, *26*, 5937–5945. [CrossRef]

67. Liu, S.; Yu, B.; Zhang, H.; Fei, T.; Zhang, T. Enhancing NO_2 gas sensing performances at room temperature based on reduced graphene oxide-ZnO nanoparticles hybrids. *Sens. Actuators B Chem.* **2014**, *202*, 272–278. [CrossRef]

68. Xia, Y.; Wang, J.; Xu, J.-L.; Li, X.; Xie, D.; Xiang, L.; Komarneni, S. Confined formation of ultrathin ZnO nanorods/reduced graphene oxide mesoporous nanocomposites for high-performance room-temperature NO_2 sensors. *ACS Appl. Mater. Interfaces* **2016**, *8*, 35454–35463. [CrossRef] [PubMed]

69. Huang, Q.; Zeng, D.; Li, H.; Xie, C. Room temperature formaldehyde sensors with enhanced performance, fast response and recovery based on zinc oxide quantum dots/graphene nanocomposites. *Nanoscale* **2012**, *4*, 5651–5658. [CrossRef] [PubMed]

70. Mu, H.; Zhang, Z.; Zhao, X.; Liu, F.; Wang, K.; Xie, H. High sensitive formaldehyde graphene gas sensor modified by atomic layer deposition zinc oxide films. *Appl. Phys. Lett.* **2014**, *105*, 033107. [CrossRef]

71. Zhang, D.; Liu, J.; Xia, B. Layer-by-layer self-assembly of zinc oxide/graphene oxide hybrid toward ultrasensitive humidity sensing. *IEEE Electron Device Lett.* **2016**, *37*, 916–919. [CrossRef]

72. Taylor, J.; Guo, H.; Wang, J. Ab initio modeling of quantum transport properties of molecular electronic devices. *Phys. Rev. B* **2001**, *63*, 245407. [CrossRef]

73. Brandbyge, M.; Mozos, J.-L.; Ordejón, P.; Taylor, J.; Stokbro, K. Density-functional method for nonequilibrium electron transport. *Phys. Rev. B* **2002**, *65*, 165401. [CrossRef]

74. Atomistix ToolKit (ATK), Version 2017.2, QuantumWise Simulator A/S. Available online: www.quantumwise.com (accessed on 9 August 2018).

75. Grimme, S. Semiempirical GGA-type density functional constructed with a long-range dispersion correction. *J. Comput. Chem.* **2006**, *27*, 1787–1799. [CrossRef] [PubMed]

76. Grimme, S.; Mück-Lichtenfeld, C.; Antony, J. Noncovalent interactions between graphene sheets and in multishell (hyper) fullerenes. *J. Phys. Chem. C* **2007**, *111*, 11199–11207. [CrossRef]

77. Pyykkö, P.; Atsumi, M. Molecular Single-Bond Covalent Radii for Elements 1–118. *Chem. A Eur. J.* **2009**, *15*, 186–197. [CrossRef] [PubMed]

78. Zhang, Y.; Gao, B.; Xu, Z. Adsorption properties of polyvinyl-alcohol-grafted particles toward genistein driven by hydrogen-bond interaction. *J. Phys. Chem. B* **2013**, *117*, 5730–5736. [CrossRef] [PubMed]

79. Yuan, Q.; Zhao, Y.-P.; Li, L.; Wang, T. Ab initio study of ZnO-based gas-sensing mechanisms: Surface reconstruction and charge transfer. *J. Phys. Chem. C* **2009**, *113*, 6107–6113. [CrossRef]

80. Casarin, M.; Tondello, E.; Vittadini, A. A LCAO-LDF study of CO and NH3 chemisorption on ZnO (0001). *Surf. Sci.* **1994**, *307*, 1182–1187. [CrossRef]

81. An, W.; Wu, X.; Zeng, X.C. Adsorption of O_2, H_2, CO, NH_3, and NO_2 on ZnO nanotube: A density functional theory study. *J. Phys. Chem. C* **2008**, *112*, 5747–5755. [CrossRef]

82. Spencer, M.J.; Yarovsky, I. ZnO nanostructures for gas sensing: Interaction of NO_2, NO, O, and N with the ZnO (1010) surface. *J. Phys. Chem. C* **2010**, *114*, 10881–10893. [CrossRef]

83. Breedon, M.; Spencer, M.; Yarovsky, I. Adsorption of NO_2 on oxygen deficient ZnO (2110) for gas sensing applications: A DFT study. *J. Phys. Chem. C* **2010**, *114*, 16603–16610. [CrossRef]

84. Ma, J.; Michaelides, A.; Alfe, D.; Schimka, L.; Kresse, G.; Wang, E. Adsorption and diffusion of water on graphene from first principles. *Phys. Rev. B* **2011**, *84*, 033402. [CrossRef]

85. Ye, H.; Chen, G.; Niu, H.; Zhu, Y.; Shao, L.; Qiao, Z. Structures and mechanisms of water adsorption on ZnO (0001) and GaN (0001) surface. *J. Phys. Chem. C* **2013**, *117*, 15976–15983. [CrossRef]

86. Meyer, B.; Rabaa, H.; Marx, D. Water adsorption on ZnO (1010): From single molecules to partially dissociated monolayers. *Phys. Chem. Chem. Phys.* **2006**, *8*, 1513–1520. [CrossRef] [PubMed]

87. Goclon, J.; Meyer, B. The interaction of H_2S with the ZnO (1010) surface. *Phys. Chem. Chem. Phys.* **2013**, *15*, 8373–8382. [CrossRef] [PubMed]

88. Ling, L.; Zhang, R.; Han, P.; Wang, B. DFT study on the sulfurization mechanism during the desulfurization of H_2S on the ZnO desulfurizer. *Fuel Process. Technol.* **2013**, *106*, 222–230. [CrossRef]

89. Ganji, M.D.; Sharifi, N.; Ardjmand, M.; Ahangari, M.G. Pt-decorated graphene as superior media for H_2S adsorption: A first-principles study. *Appl. Surf. Sci.* **2012**, *261*, 697–704. [CrossRef]

90. Rodriguez, J.A.; Maiti, A. Adsorption and decomposition of H_2S on MgO (100), NiMgO (100), and ZnO (0001) surfaces: A first-principles density functional study. *J. Phys. Chem. B* **2000**, *104*, 3630–3638. [CrossRef]

91. Zhang, Y.-H.; Yue, L.-J.; Gong, F.-L.; Li, F.; Zhang, H.-L.; Chen, J.-L. Highly enhanced H_2S gas sensing and magnetic performances of metal doped hexagonal ZnO monolayer. *Vacuum* **2017**, *141*, 109–115. [CrossRef]

92. Song, H.S.; Park, M.G.; Kwon, S.J.; Yi, K.B.; Croiset, E.; Chen, Z.; Nam, S.C. Hydrogen sulfide adsorption on nano-sized zinc oxide/reduced graphite oxide composite at ambient condition. *Appl. Surf. Sci.* **2013**, *276*, 646–652. [CrossRef]

93. Cuong, T.V.; Pham, V.H.; Chung, J.S.; Shin, E.W.; Yoo, D.H.; Hahn, S.H.; Huh, J.S.; Rue, G.H.; Kim, E.J.; Hur, S.H. Solution-processed ZnO-chemically converted graphene gas sensor. *Mater. Lett.* **2010**, *64*, 2479–2482. [CrossRef]

94. Liu, X.; Sun, J.; Zhang, X. Novel 3D graphene aerogel–ZnO composites as efficient detection for NO_2 at room temperature. *Sens. Actuators B Chem.* **2015**, *211*, 220–226. [CrossRef]

95. Song, H.S.; Park, M.G.; Ahn, W.; Lim, S.N.; Yi, K.B.; Croiset, E.; Chen, Z.; Nam, S.C. Enhanced adsorption of hydrogen sulfide and regeneration ability on the composites of zinc oxide with reduced graphite oxide. *Chem. Eng. J.* **2014**, *253*, 264–273. [CrossRef]